Available online at www.sciencedirect.com

ScienceDirect

Geochimica et Cosmochimica Acta 285 (2020) 207–224

Geochimica et Cosmochimica Acta

www.elsevier.com/locate/gca

Chromium reduction and associated stable isotope fractionation restricted to anoxic shelf waters in the Peruvian Oxygen Minimum Zone

Philipp Nasemann [a,*], David J. Janssen [a], Jörg Rickli [a,b], Patricia Grasse [c], Martin Frank [c], Samuel L. Jaccard [a]

[a] *Institute of Geological Sciences and Oeschger Center for Climate Change Research, University of Bern, Baltzerstrasse 1-3, CH-3012, Switzerland*

[b] *Institute of Geochemistry and Petrology, ETH Zürich, Clausiusstrasse 25, CH-8092, Switzerland*

[c] *GEOMAR Helmholtz Centre for Ocean Research Kiel, Wischhofstrasse 1-3, D-24148, Germany*

Received 19 August 2019; accepted in revised form 24 June 2020; available online 3 July 2020

Abstract

The marine chromium (Cr) cycle is still insufficiently understood, in particular the mechanisms modulating the spatial distribution of dissolved stable Cr isotopes in seawater. Redox transformations between its main oxidation states, Cr(VI) and Cr(III), have been held accountable for the observed tight inverse logarithmic relationship between the dissolved Cr concentration [Cr] and its isotopic composition (δ^{53}Cr), whereby isotopically light Cr(III) is removed in surface waters and oxygen minimum zones (OMZs), and subsequently released to deeper waters from remineralized particles or sediments.

Seawater [Cr] and δ^{53}Cr were investigated in a series of depth profiles across the Peruvian margin OMZ, covering a wide spectrum of dissolved oxygen concentrations ranging from 2 to 242 μmol/kg. We found [Cr] ranging from 1.5 to 5.5 nmol/kg, associated with δ^{53}Cr variations between +1.59 and +0.72‰, but no systematic relationship to dissolved oxygen concentrations. However, distinctly different seawater profiles were observed above the suboxic/anoxic shelf compared to those located further offshore, with substantial Cr removal restricted to suboxic or anoxic environments on the shelf. This suggests that suboxic conditions ($[O_2] < 5$ μmol/kg) alone are not sufficient to account for substantial Cr removal. Given that environmental conditions under which Cr can be reduced remain restricted spatially, the role of this sink in the marine Cr cycle may therefore be small. Additionally, some observations corroborate the assumption that Cr reduction is not necessarily accompanied by immediate adsorption of the formed Cr(III) onto particles, leading to its removal from the dissolved phase. Instead, partial removal of Cr(III) via particles, leaving a residual dissolved Cr(III) pool, may be more widespread in suboxic waters.

Keywords: Chromium isotopes; Oxygen minimum zones

1. INTRODUCTION

The chromium (Cr) stable isotope system has received growing attention since Cr isotope fractionation has been linked to redox transformations between its main oxidation states Cr(VI) and Cr(III) (Ball and Bassett, 2000). Stable Cr isotope systematics have thus been applied to reconstruct past variations in the redox state of Earth's atmosphere and oceans (e.g. Frei et al., 2009; Reinhard et al., 2014; Planavsky et al., 2014; Cole et al., 2016; Holmden et al., 2016; Canfield et al., 2018). However, the marine Cr cycle is still insufficiently understood, in particular the

* Corresponding author.
E-mail address: philipp.nasemann@geo.unibe.ch (P. Nasemann).

https://doi.org/10.1016/j.gca.2020.06.027
0016-7037/

mechanisms modulating the spatial distribution of dissolved stable Cr isotopes in seawater.

1.1. Cr distribution and speciation in seawater

In unpolluted seawater, Cr is present as a dissolved trace element at concentrations ranging from ~0.9 to 6.5 nmol/kg (Campbell and Yeats, 1981; Cranston, 1983; Jeandel and Minster, 1984; Sirinawin et al., 2000; Connelly et al., 2006; Bonnand et al., 2013; Scheiderich et al., 2015; Goring-Harford et al., 2018; Moos and Boyle, 2019). Estimates of its oceanic residence time vary widely, reflecting the uncertainties associated with the marine Cr cycle, and range from ~3000 to 45,000 years (Campbell and Yeats, 1981; Quinby-Hunt and Turehian, 1983; Whitfield and Turner, 1987; Reinhard et al., 2014; Qin and Wang, 2017). Under well-oxygenated conditions, the more soluble and weakly adsorbing Cr(VI) species generally accounts for >70% of dissolved Cr and forms a chromate oxyanion, CrO_4^{2-}. However, owing to the high redox potential of the Cr(VI)/Cr(III) couple, the reduction of Cr(VI) is more easily achieved than the kinetically much slower back-oxidation, which usually results in the presence of some reduced Cr(III) forming insoluble, particle-reactive hydroxide complexes (such as $Cr(OH)_2^+$ and $Cr(OH)_3$) (Elderfield, 1970; Achterberg and van den Berg, 1997; Sirinawin et al., 2000). Because Cr(III) hydroxide complexes are efficiently scavenged onto Fe(III) oxyhydroxides, Cr reduction represents the main Cr removal pathway from the dissolved phase (Elderfield, 1970; Cranston and Murray, 1978; Rai et al., 1989) although mechanisms maintaining Cr(III) in solution through complexation with organic ligands have been identified (Sander and Koschinsky, 2000; Saad et al., 2017). Chromium reduction may be catalyzed by reducing agents, such as organic matter, H_2O_2, and Fe(II) in oxic waters, or facilitated under reducing conditions in the water column (Achterberg and van den Berg, 1997; Pettine, 2000; Connelly et al., 2006; Li et al., 2009; Zink et al., 2010; Døssing et al., 2011).

Connelly et al. (2006) reported that Cr(III) concentrations were significantly correlated with biological activity and bacterial biomass in the Sargasso Sea and Janssen et al. (2020) demonstrated correlation with net community productivity and maxima in highly productive surface waters. Both studies suggest that carbon export may provide an important removal term of Cr from the upper ocean. Accordingly, Cr(III) can temporarily account for up to 50% of total dissolved Cr in surface waters (Connelly et al., 2006). Previous studies found that Cr may be incorporated into plankton biomass, although it apparently does not engage in any biochemical functions (Mayer, 1988). Semeniuk et al. (2016) reported extracellular adsorption and, to a lesser degree, direct incorporation of Cr(III) by phytoplankton, which could be the key mechanism to explain observed surface water Cr depletion supporting a major role for the biological carbon pump in regulating global seawater dissolved Cr distribution patterns.

The removal of Cr from seawater may also take place in areas where the reduction of Cr(VI) can be catalyzed, such as in oxygen minimum zones (OMZs). These zones occur at intermediate depths along eastern boundary upwelling systems as a result of high primary productivity and oxygen consumption upon decomposition of sinking organic particles combined with sluggish O_2 replenishment by ocean circulation (e.g. Karstensen et al., 2008). Water-column profiles in OMZs accordingly show maxima in dissolved Cr(III) and particulate Cr concentrations, coinciding with dissolved Cr(VI) minima at the lowest dissolved oxygen levels <5 μmol/kg (Murray et al., 1983; Rue et al., 1997).

Owing to removal from surface waters and subsequent remineralization at depth, Cr concentrations are typically elevated in deeper waters. Inputs from rivers, thought to be the major input term of Cr to the oceans (Jeandel and Minster, 1987), or the atmosphere can, however, cause high surface ocean Cr concentrations locally (Achterberg and van den Berg, 1997). Similarly, hydrothermal sources and diffusion from marine sediments can explain high Cr concentrations close to the seabed (e.g. Campbell and Yeats, 1981; Cranston, 1983; Jeandel and Minster, 1984; Jeandel and Minster, 1987; Achterberg and Van Den Berg, 1997; Sander and Koschinsky, 2000). In the absence of external inputs or removal mechanisms, Cr concentrations likely simply reflect those of newly formed water masses subducted into the ocean interior and mixing between different water masses, which will also control the Cr isotope distribution (Sirinawin et al., 2000; Scheiderich et al., 2015; Rickli et al., 2019).

1.2. Cr isotopes in seawater

Reported seawater chromium stable isotopes ($\delta^{53}Cr$) values range between +0.41 and +1.72‰ (Bonnand et al., 2013; Paulukat et al., 2015; Scheiderich et al., 2015; Holmden et al., 2016; Paulukat et al., 2016; Frei et al., 2018; Goring-Harford et al., 2018; Farkaš et al., 2018; Moos and Boyle, 2019; Rickli et al., 2019; Janssen et al., 2020), which is consistently heavier than silicate rocks (-0.124 ± 0.101‰; Schoenberg et al., 2008) and thought to result from redox cycling of weathering-released Cr during riverine transport (e.g. Frei et al., 2009; Crowe et al., 2013; Frei et al., 2014; Planavsky et al., 2014; Paulukat et al., 2015). Detailed oceanic depth profiles of $\delta^{53}Cr$ are still scarce and restricted to a few stations in the Arctic Ocean (Scheiderich et al., 2015), the North Pacific (Moos and Boyle, 2019; Janssen et al., 2020), the Southern Ocean (Rickli et al., 2019) and the Atlantic (Bonnand et al., 2013; Goring-Harford et al., 2018). The scarcity of data impedes further unravelling of the processes associated with the internal cycling of Cr in the oceans. It has been proposed that the Cr isotopic composition of seawater is principally controlled by coupled Cr(VI) reduction and Cr(III) removal in surface waters and OMZs and Cr(VI) input from remineralized particles or sediments at depth (Scheiderich et al., 2015; Janssen et al., 2020). This is reflected by a tight inverse logarithmic relationship between the dissolved Cr concentration [Cr] and its isotopic composition $\delta^{53}Cr$, referred to as the 'global trend line' (Scheiderich et al., 2015). Theoretical and experimental studies have indeed shown that reduction of Cr(VI) imposes isotope fractiona-

tion associated with preferential partitioning of the light ^{52}Cr into the reduced Cr(III) species, whereby the residual Cr(VI) becomes relatively enriched in ^{53}Cr (Schauble, 2004; Zink et al., 2010; Døssing et al., 2011). The empirically determined isotope fractionation linked to the observed $\delta^{53}Cr$-ln([Cr]) correlation ($\varepsilon_{Cr(III)-Cr(VI)} = -0.8 \pm 0.03‰$; Scheiderich et al., 2015) is relatively small when compared to experimentally derived fractionation factors associated with Cr reduction by H_2O_2 (−5‰; Zink et al., 2010) or Fe(II) (up to −4.53‰; Døssing et al., 2011). Currently, it remains unclear whether low oxygen concentrations in the water column alone may prompt Cr reduction. Goring-Harford et al. (2018) and Moos et al. (2020) found no correlation between dissolved oxygen and Cr concentrations, or isotopic composition under dysoxic (dissolved oxygen 44–90 μmol/kg) and even more reducing (dissolved oxygen <2 μmol/kg) conditions.

In order to investigate in more detail whether low oxygen concentrations may facilitate Cr reduction and to determine whether there is a threshold O_2 value for a thermodynamic response of Cr, we investigate stable Cr isotope fractionation in seawater samples from the Peruvian upwelling region. Samples derive from 10 stations offshore Peru, along the continental slope and on the shelf that altogether cover a wide range of dissolved oxygen concentrations (<2–242 μmol/kg) and different biogeochemical conditions.

2. STUDY AREA

The Peruvian coastal upwelling region features one of the highest rates of primary and export production in the global ocean (Bruland et al., 2005; Pennington et al., 2006). Persistent easterly trade and alongshore winds foster offshore Ekman transport of surface waters, which are replaced by upwelling of oxygen-depleted, nutrient-rich subsurface waters that represent the main supply of dissolved phosphate (PO_4^{3-}), silicic acid ($Si(OH)_4$), and iron (Fe) to the surface ocean ecosystem (Bruland et al., 2005; Abrantes et al., 2007; Franz et al., 2012; Ehlert et al., 2012; Grasse et al., 2016). Upwelled water is mostly sourced from two southward flowing subsurface currents, the Peru-Chile Countercurrent (PCCC) and the Peru-Chile Undercurrent (PCUC) that prevail between 50 and 150 m water depth (Fig. 1), as well as the Peru Coastal Current (PCoastalC), flowing northward at the surface (Wyrtki, 1967; Brink et al., 1983; Toggweiler et al., 1991; Penven et al., 2005; Fiedler and Talley, 2006; Silva et al., 2009). Flowing closest to shore, the PCUC is the main current influencing the northern and central Peruvian shelf before joining with the PCCC at around 14°S (Czeschel et al., 2011).

Upwelling and biological productivity were highest between 5 and 15°S during the sampling period of this study (Ehlert et al., 2012). The magnitude of primary productivity off Peru is so high that the associated decomposition (bacterial respiration) of sinking organic matter effectively consumes most of the available oxygen in the water column, resulting in one of the most pronounced oxygen minimum zones (OMZs) of the world's ocean, with oxygen levels often below 5 μmol/kg (Karstensen et al., 2008; Fuenzalida et al., 2009; Thamdrup et al., 2012). Consistent with upwelling intensity and productivity, the OMZ was most pronounced along the coastline of northern and central Peru between 5 and 15°S extending from approximately 50–700 m water depth (Karstensen et al., 2008; Fuenzalida et al., 2009). These latitudes also host a wide shelf area (~150 km wide) characterized by high benthic nutrient supply, contributing to release Fe from oxygen-deficient shelf sediments (Bruland et al., 2005; Scholz et al., 2014). The shelf of southern Peru (south of 14°S), however, is less than 10 km wide in parts, resulting in dissolved bottom water Fe concentrations an order-of-magnitude lower than observed further north (Bruland et al., 2005). Due to enhanced remineralization within the

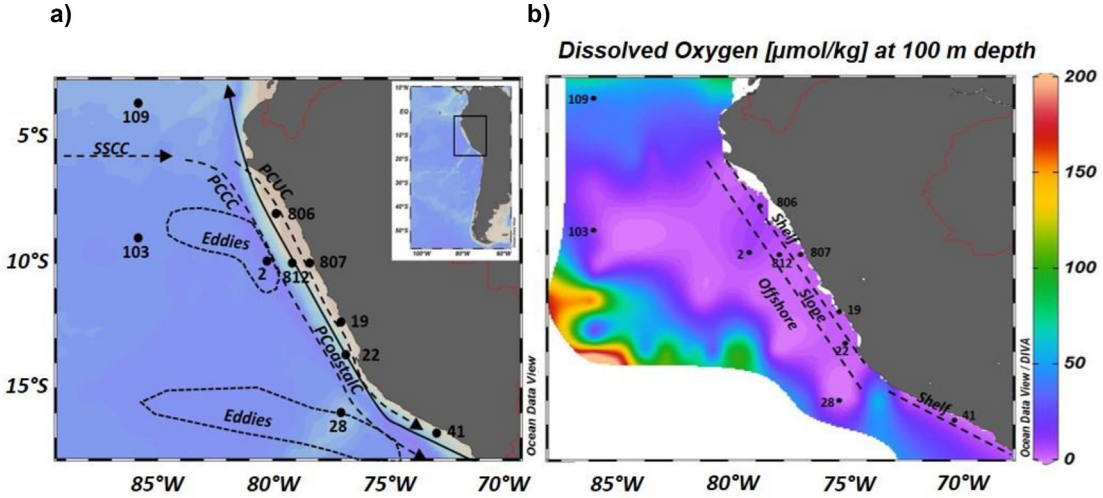

Fig. 1. Overview of the study area: a) Sampling stations and local currents as described in Czeschel et al. (2011). The most relevant surface (solid black lines) and subsurface (dashed black lines) currents are: Southern Subsurface Counter current (SSCC), Peru-Chile Countercurrent (PCCC), Peru-Chile Undercurrent (PCUC), Peru Coastal Current (PCoastalC). b) Dissolved oxygen at 100 m in the Peru OMZ and visualization of the three different sampling settings, shelf, slope and offshore.

OMZ and processes at the seawater-sediment boundary, the biogeochemical properties of the PCUC are continuously modified during southward flow (e.g. Bruland et al., 2005).

3. METHODS

3.1. Sample collection

Samples for this study were collected during legs 3 and 4 of research cruise M77 with RV Meteor between the end of December 2008 and January 2009 when seasonal primary productivity was most intense (austral summer). Sampling locations include depth profiles along the Peruvian shelf (St. 19, 41, 806 and 807) and continental slope (St. 22 and 812) down to 300 m depth, as well as offshore casts (St. 2, 28, 103 and 109), down to 4000 m (Fig. 1). Water samples were collected with Niskin bottles attached to a Rosette equipped with a Seabird CTD and oxygen sensors. Oxygen concentrations were later calibrated with bottle oxygen data measured by Winkler titration (Winkler, 1888). Samples were immediately filtered through pre-cleaned 0.45 μm pore size, nitrocellulose acetate filters (Millipore, U.S.A.) upon recovery and collected in acid cleaned LDPE bottles (Nalgene, U.S.A.). Following filtration, the samples were acidified to pH < 2 with concentrated Teflon-distilled HCl (1 ml of 10 M HCl per litre of seawater) (Ehlert et al., 2012) promoting release of Cr from organics and reducing Cr(VI) to Cr(III). Under these conditions and considering the long storage time, quantitative reduction of Cr occurred long before sample processing for Cr commenced in 2018 (Jeandel and Minster, 1987; Semeniuk et al., 2016). Samples were stored at room temperature.

3.2. Analytical methods

Extraction and purification of Cr from seawater samples as well as subsequent isotopic analyses were carried out at the Institute of Geological Sciences, University of Bern, following protocols adapted from Rickli et al. (2019). All sample processing equipment was rigorously acid cleaned before use following standard protocols. Ultra-high purity acids prepared in-house through sub-boiling distillation and >18.2 MΩ de-ionized water (Milli-Q Element purification system, Millipore, U.S.A) were used throughout. Ammonia solution and hydrogen peroxide (UpA grade) were purchased from Romil (UK).

As detailed in Rickli et al. (2019), the measurement of Cr concentrations and $\delta^{53}Cr$ includes (i) an initial Cr concentration determination on 30 ml sample aliquots by isotope dilution following spiking with 0.2 ml of 5 ppb ^{50}Cr, (ii) the addition of an adjusted amount of ^{50}Cr-^{54}Cr double spike to the seawater samples processed for $\delta^{53}Cr$ (500–1500 ml), (iii) the enrichment of Cr from seawater using $Mg(OH)_2$-coprecipitation, (iv) a two-step ion chromatography to isolate Cr and (v) the mass spectrometric determination of final Cr concentrations and $\delta^{53}Cr$. The reported Cr concentrations are based on the double-spike data.

In contrast to the observations reported by Rickli et al. (2019), the samples of this study tended to produce large Mg-precipitates. In order to minimize the size of the resulting precipitates, the added volume of ammonia was kept as low as possible, usually at 6–7 ml. However, certain samples required additional ammonia subsequently added in small increments (see also Moos and Boyle, 2019). Small precipitates were generally more convenient to dissolve and prepare for anion chemistry. Some samples formed residues of silicate gel upon dissolution of the $Mg(OH)_2$ pellets in 6.4 M HCl. These were carefully separated by centrifugation and digested in a mixture of 6.4 M HCl and 0.5 M HF. Initial test analyses of digest solutions revealed that no Cr was incorporated into the residues (data not shown), which were therefore discarded.

The oxidation step of the Mg-precipitates with H_2O_2 described in Rickli et al. (2019), aimed at removing organic compounds prior to chromatography, was only performed for a third of the samples reported here. Overall, this treatment did not substantially improve the procedural yields (not shown) but carried a risk of lowering the efficiency of Cr oxidation with ammonium-persulfate (APS) in preparation for the anion exchange column (Moos and Boyle 2019). To lower the procedural blank, we halved the added APS to 1 ml of 0.1 M per sample, which is sufficient to fully oxidize Cr(III) to Cr(VI) (Janssen et al., 2020). Elution of Cr from the anion column included H_2O_2 (1 M HNO_3 + 2% v/v 30% H_2O_2) to assist with the reduction of Cr(VI) to Cr(III) (e.g. Larsen et al., 2016; Moos and Boyle, 2019).

In contrast to Rickli et al. (2019), we did not dry down the eluate of the anion column, which was instead stored for 5 days at room temperature before commencing the second purification step. This assists quantitative conversion to the Cr^{3+} free cation (Larsen et al., 2016) and should increase Cr recoveries for the subsequent purification utilizing a cation column with AG50W-X8 resin (200–400 mesh) (Yamakawa et al., 2009; Larsen et al., 2016). With the reported amendments, Cr yields have stabilized between 50% and 77%, with an average of 63%, while blanks were lowered to 8–12 pmol Cr (n = 4).

Preliminary Cr concentrations, as well as final Cr concentrations [Cr] and stable isotope compositions ($\delta^{53}Cr$) were measured on a Neptune Plus MC-ICP-MS (Fisher Scientific) following the methodology described in Rickli et al (2019). Internal precision on $\delta^{53}Cr$ was typically 0.02–0.03‰ for 100 ppb NIST 979 solutions (2SE), identical to the external reproducibility of 0.02–0.03‰ (2SD, n ≥ 11). Given that there was no drift in NIST 979 measurements during the sessions, the session's average deviation from zero (≤0.02‰) was used to adjust sample values.

Each series of 10 samples was accompanied by a procedural replicate of OSIL Atlantic Standard Seawater. Internal precision on $\delta^{53}Cr$ was typically 0.02–0.03‰ (2SE), while external reproducibility within one OSIL batch was slightly higher at 0.04‰ (2SD, n = 3). Internal precision for sample measurements was mostly in the same range as for OSIL waters and NIST 979, with some higher internal errors associated with small beams (max. 0.07‰, 2SE at 2.7 V on the ^{52}Cr beam; Table 1). A more detailed account of analytical uncertainty associated with the used method is provided in Janssen et al. (2020). Based on this, the error on

Table 1
Seawater temperature, salinity and nutrient concentration data from RV Meteor cruises M77/3 and M77/4, as well as Cr concentrations and $\delta^{53}Cr$ data.

Station	Longitude [°W]	Latitude [°S]	Depth [m]	Temperature [°C]	Salinity [PSU]	Oxygen [µmol/kg]	Potential Density [kg/m^3]	NO_3^- [µmol/kg]	NO_2^- [µmol/kg]	$Si(OH)_4$ [µmol/kg]	[Fe][c] [nmol/kg]	[Cr] [nmol/kg]	$\delta^{53}Cr$ [‰]	2SE[d] [‰]
2	80.224	9.922	2	23.60	35.26	219.8	23.96	5.19	0.11	0.35		2.94	1.09	0.03
2			102 [b]	14.60	35.02	4.6	26.08	30.23	0.03	17.02		3.09	1.16	0.03
												3.09	1.14	0.02
2			999	4.57	34.52	49.5	27.38	49.15	-	-		4.23	0.86	0.03
19	77	12.363	2	19.64	34.89	191.4	24.72	2.34	1.05		82.85	2.14	0.92	0.02
19			97 [b]	13.72	34.97	2.0	26.23	0.13	0.05		188.13	2.17	1.00	0.05
												2.17	1.08	0.05
22	76.785	13.666	3	17.20	34.93	211.7		8.16	0.51			2.55	1.16	0.02
22			153	13.02	34.94	2.0		11.79	8.63			2.70	1.30	0.02
22			302	11.69	34.85	2.2		21.23	5.62			3.05	1.18	0.02
28	76.998	15.999	8	23.24	35.30	206.4	24.10	0.03	0.02	1.04	1.25	2.93	1.07	0.04
28			201	12.18	34.88	2.1	26.47	-	-	-	2.26	2.86	1.25	0.03
28			1001 [a]	4.58	34.53	47.8	27.37	-	-	-		4.26	0.88	0.03
												4.36	0.90	0.03
28			1800 [a]	2.55	34.63	91.2	27.65	-	-	-		4.86	0.79	0.03
												5.02	0.79	0.05
41	72.841	16.819	2	21.17	34.95	242.0	24.41	0	7.08			2.91	1.06	0.07
41			100	12.86	34.89	2.0	26.35	12.63	6.45			2.52	1.24	0.04
41			250	12.30	34.87	2.3	26.45	13.87	7.77			2.54	1.14	0.05
103	85.833	9	2	26.75	35.52	215.5	23.19	2.76	-	0.77		2.96	1.11	0.02
103			151	13.06	34.95	10.7	26.35	30.89	-	21.54		3.22	1.09	0.02
103			221	12.34	34.91	33.6	26.46	29.41	-	21.74		3.30	1.08	0.02
103			800 [a]	5.53	34.55	34.0	27.27	45.26	-	66.41		3.95	0.92	0.03
												3.94	0.89	0.03
103			1500	2.96	34.61	83.2	27.59	41.26	-	121.64		4.68	0.80	0.03
103			2501	1.92	34.67	118.3	27.74	38.17	-	147.57		5.22	0.73	0.02
103			4290	1.81	34.69	146.5	27.77	35.86	-	138.86		5.51	0.72	0.02
109	85.833	3.583	2	25.49	34.49	215.0	22.81	6.33	-	1.03		3.04	1.11	0.02
109			151	13.53	34.96	46.4	26.27	27.64	-	19.57		3.31	1.03	0.03
109			500	8.18	34.64	8.6	26.96	40.64	-	46.14		3.51	1.15	0.02
109			700	6.28	34.58	22.1	27.19	44.72	-	61		3.80	0.97	0.02
109			1500	3.24	34.61	80.0	27.57	40.83	-	118.06		4.56	0.83	0.02
109			3201	1.78	34.68	134.3	27.76	37.09	-	143.63		5.29	0.73	0.02
806	79.845	8	1	19.39	34.99	212.8	24.92	6.75	0.55			2.31	1.02	0.04
806			81	14.08	34.99	9.1	26.17	31.49	0.06			3.28	1.05	0.04
806			141	13.74	34.97	2.1	26.23	14.71	9.02			1.50	1.59	0.03
807	78.380	10.001	2	16.38	35.00	65.5	25.54	20.87	1.77		2.44	2.57	1.17	0.03
807			80 [b]	13.65	34.97	2.0	26.23	1.92	10.75		30.44	1.71	1.41	0.03
												1.71	1.43	0.02
807			110 [b]	13.65	34.97	2.0	26.23	1.68	10.51			1.67	1.49	0.04
												1.67	1.52	0.02
812	79.134	9.999	3	21.85	35.13	225.0	24.36	5.57	0.22			2.53	1.11	0.03

812	51 [b]	14.59	35.00	13.7	26.06	30.51	0.07	3.21	0.98	0.04
								3.21	1.00	0.02
812	101 [b]	13.65	34.98	3.7	26.25	32.29	0.03	3.23	1.06	0.03
								3.23	1.08	0.02
812	201	12.89	34.93	2.0	26.37	31.65	0.16	3.09	1.13	0.03
812	302	11.78	34.86	2.2	26.53	29.48	2.56	3.05	1.19	0.02
OSIL	Saskatchewan Isotope Laboratory (16/9/2015)							3.24	0.95	0.02
OSIL	University of Bern (5/12/2017), Bottle 2 [a]							4.17	0.81	0.03
	[a]							4.16	0.81	0.03
								4.18	0.80	0.03

[a] Processed replicate - a separate seawater aliquot of a sample was processed through the entire sample treatment protocol.
[b] Replicate measurement - a single seawater sample was processed once through the sample treatment protocol, but measured twice.
[c] From Schlosser et al. (2018).
[d] Represents the internal error of a sample measurement.

isotope compositions is 0.03–0.04‰ (2 SD) and <1% for [Cr] (1 SD).

The chromium isotope composition is expressed as the deviation of the $^{53}Cr/^{52}Cr$ ratio relative to the NIST SRM 979 standard in δ notation.

$$\delta^{53}Cr\ [\%] = \left(\left({}^{53}Cr/{}^{52}Cr \right)_{Sample} / \left({}^{53}Cr/{}^{52}Cr \right)_{NIST\ 979} - 1 \right) \times 1000$$

4. RESULTS

Dissolved Cr concentrations vary from 1.5 to 5.5 nmol/kg, while the total range of $\delta^{53}Cr$ values spans from +0.72 to +1.59‰ (Table 1). The most homogeneous Cr pools are surface (0–10 m) and deep waters (>1000 m), whereas [Cr] and $\delta^{53}Cr$ vary at intermediate depths.

Surface water concentrations (2.14–3.04 nmol/kg) follow no systematic trend along the shelf but increase slightly towards the stations furthest offshore, whereas isotopic compositions (ranging from +0.92 to +1.17‰) do not vary systematically in space. Offshore stations (2, 28, 103 and 109) are identical within analytical error in both [Cr] and $\delta^{53}Cr$ (Fig. 2g–j; Table 1), whereas slope (Fig. 2 e & f) and shelf (Fig. 2 a-d) stations range between 2.14 and 2.91 nmol/kg Cr and +0.92 and +1.17‰. The upper 10 m of the water column are also the most oxygenated in the study area, with dissolved oxygen ≥200 µmol/kg. The depth of the oxycline, where dissolved oxygen concentrations abruptly decrease, varies between 20 m and 100 m, closely following a potential density of ~26.1 kg/m^3. It is shallowest on the shelf and deepest offshore at stations 2 and 28 (~90 m), which were located in areas with high eddy activity at the time of sampling (Czeschel et al., 2011; Grasse et al., 2016).

Vertical distributions of [Cr] and $\delta^{53}Cr$ are systematically different between offshore and shelf stations. Offshore stations show gradually increasing [Cr] and decreasing $\delta^{53}Cr$ with depth (Fig. 2g–j), consistent with the patterns described in open ocean settings elsewhere (Scheiderich et al., 2015; Moos & Boyle, 2019; Rickli et al., 2019; Janssen et al., 2020). Their deep waters (>1000 m) feature Cr concentrations between 4.56 and 5.51 nmol/kg, while $\delta^{53}Cr$ ranges from +0.72 to +0.83‰. Closer to the continental slope, where the water depth is much shallower, [Cr] and $\delta^{53}Cr$ depth gradients are smaller, only reaching 3.05 nmol/kg and ~ +1.19‰ approaching the seabed (stations 812 and 22; Fig. 2e–f). Stations above the shelf, in contrast, display the lowest [Cr] (1.50–1.67 nmol/kg) and heaviest $\delta^{53}Cr$ values (+1.51 to +1.59‰; stations 806 and 807 respectively; Fig. 2a/b) at ~100–150 m, near the seafloor, where suboxic conditions ($[O_2] < 5$ µmol/kg) prevail.

5. DISCUSSION

Plotted in a $\delta^{53}Cr$-ln([Cr]) diagram, our data follow the global trend line defined by previously published data, with only three points plotting slightly below the line (Fig. 3). Although the global trend line including our data yields a slightly smaller fractionation factor (−0.70 ± 0.08‰) than

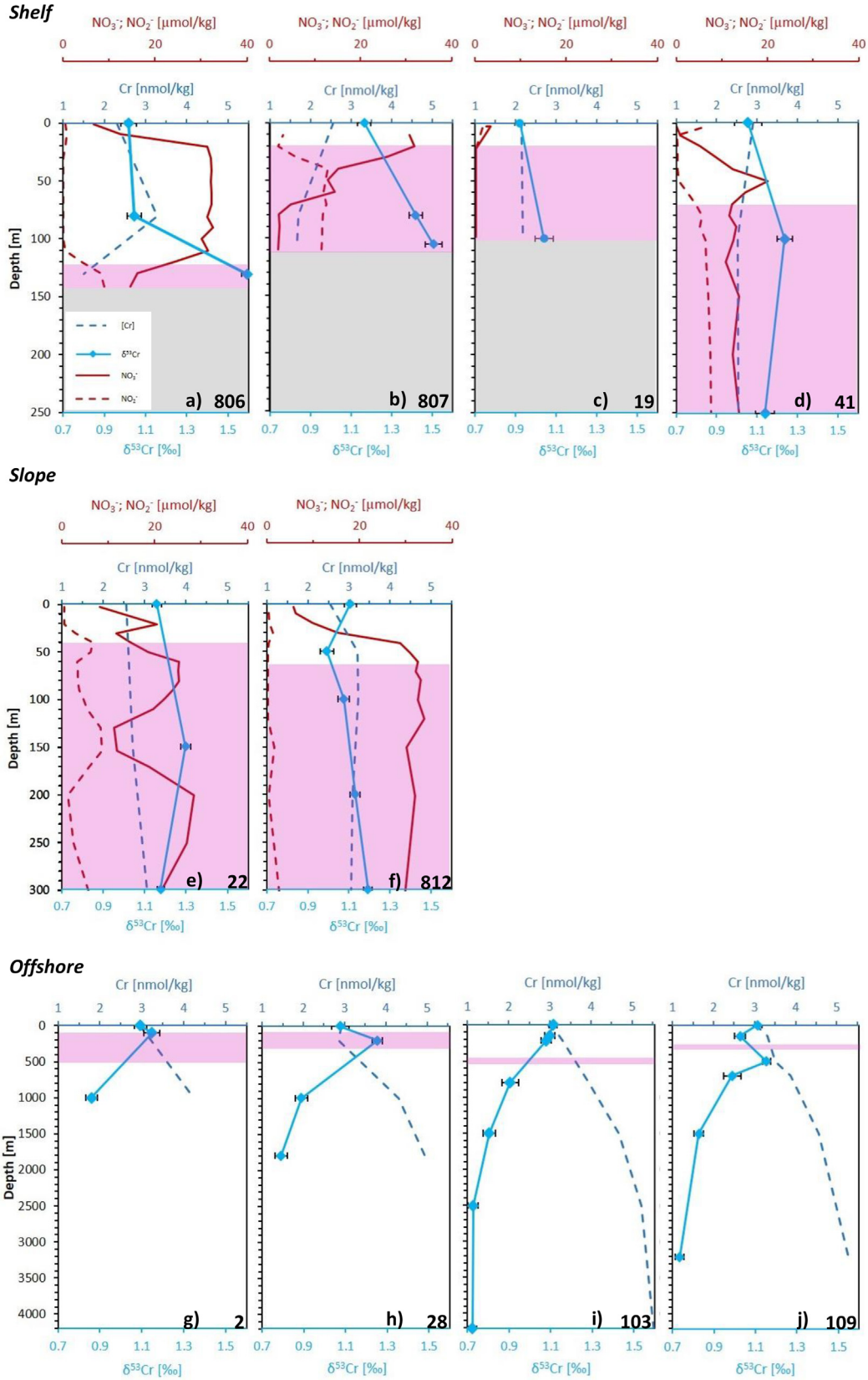

Fig. 2. Depth profiles showing the vertical distribution of Cr concentrations, $\delta^{53}Cr$, as well as nitrate (NO_3^-) and nitrite (NO_2^-) (only for shelf and slope stations). For better visibility, Cr data is displayed with lines connecting data points. These do not represent the true depth distribution. [Cr] datapoints are located at equal depths as $\delta^{53}Cr$ datapoints. Error bars on $\delta^{53}Cr$ are 2SE for single measurements. In case of replicate measurements (or processed replicates), an average value was plotted and error bars either represent external reproducibility (0.033‰) or the internal error, whichever was higher (see also Table 1). The purple shaded areas mark suboxic/anoxic water depths.

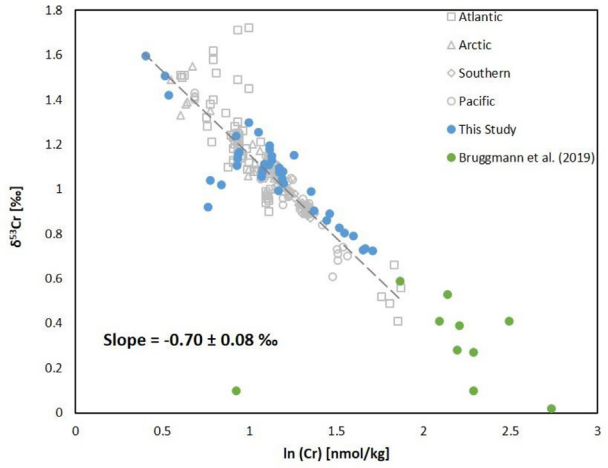

Fig. 3. δ^{53}Cr versus ln ([Cr]) for the new data from this study and previous publications of open ocean data sets: Bonnand et al., 2013, Scheiderich et al. (2015), Goring-Harford et al. (2018), Moos and Boyle (2019), Rickli et al. (2019) and Janssen et al., (2020). Small-scale data sets focusing solely on surface waters or such with contaminated seawater (Economou-Eliopoulos et al., 2016) were excluded as well as surface mixed layer samples from the Scheiderich dataset, which were diluted by sea ice or river water. Data from Bruggmann et al. (2019) are included in the plot but not the regression.

previous publications (-0.82 ± 0.06‰; e.g. Rickli et al., 2019; Janssen et al., 2020), the values overlap within uncertainty. Chromium concentrations are within the spectrum of previously published open ocean [Cr] data (e.g. Jeandel and Minster, 1987; Rue et al., 1997; Connelly et al., 2006; Scheiderich et al., 2015; Goring-Harford et al., 2018; Moos and Boyle, 2019; Rickli et al., 2019; Janssen et al., 2020) and the reported Cr isotopic compositions essentially encompass the range of most global seawater data available to date (Scheiderich et al., 2015; Goring-Harford et al., 2018; Moos and Boyle, 2019; Rickli et al., 2019; Janssen et al., 2020), Fig. 3). However, our concentrations are significantly lower than recently published [Cr] for two seawater profiles from 245 m (shelf) and 2022 m (open ocean) depth off Peru (12–13°S) by Bruggmann et al. (2019). These published data generally cluster between 8 and 9 nmol/kg with extreme values reaching 2.5 and 15.4 nmol/kg (Bruggmann et al., 2019), and our δ^{53}Cr data do not overlap with these data. However, the close spatial proximity of sampling stations suggests that these data should be similar. We provide a summarized assessment of these differences in terms of analytical methodology, intercalibration, the concept of "oceanographic consistency" (Boyle et al., 1977), and sediment dynamics, with a detailed discussion presented in the supplemental material.

Methodology: Methodological differences between both studies include sampling systems, filter types and pore size, sample storage time and preconcentration technique. Neither differences in rosette type (Scheiderich et al., 2015), nor in filter pore size should influence [Cr] (e.g. Goring-Harford et al., 2018, which used both, 0.45 and 0.2 µm). While polyethersulfone (SUPOR) filters as used by Bruggmann et al. (2019) have substantial Cr blanks (Scheiderich et al., 2015), it appears that no Cr is mobilized from the membrane during seawater filtration (e.g. Scheiderich et al., 2015; Goring-Harford et al., 2018; Rickli et al., 2019; Janssen et al., 2020). There is no systematic trend in [Cr] among recent Cr isotope studies with variable sample storage time (Moos and Boyle, 2019: ~8 years; Goring-Harford et al., 2018: ~6 years; Scheiderich et al., 2015: ~5 years; Rickli et al., 2019: 1 year), where the data of Bruggmann et al. (2019) (~4 years storage time) yield generally much higher [Cr]. Therefore, differences in sampling or sample storage do not seem to explain the differences we see between our data and those of Bruggmann et al. (2019).

Our study employed Mg co-precipitation, which has undergone rigorous testing in lab and field samples to confirm that it provides quantitative determination of [Cr] following sample-spike equilibration (Semeniuk et al., 2016; Moos & Boyle, 2019; Rickli et al., 2019; Davidson et al., 2020), including potential organically-complexed Cr (Davidson et al., 2020). Additionally, we validated our method in terms of concentration and isotope composition through an inter-comparison with the Saskatchewan Isotope Laboratory (Rickli et al. 2019). This supports that our method is accurate, whereas the evaporation approach used by Bruggmann et al., (2019) which will not remove any sample matrix prior to chemical processing, has not yet undergone the same lab testing nor any intercalibration exercise.

Oceanographic Consistency: This was the initially established concept to gauge data quality, when the first uncontaminated data of many metals were reported (Boyle et al., 1977). The fundamental principles are that "detailed profiles should show smooth variations related to the hydrographic and chemical features displayed by conventionally measured properties. Regional variations should be compatible with what is known of the large-scale physical and chemical circulation of the oceans." (Boyle et al., 1977). Hence, depth profiles of [Cr] or δ^{53}Cr should be relatively smooth and relatable to known processes such as biological uptake, regeneration, scavenging, circulation and sedimentary Cr release. Our data follow these criteria (see Sections 5.1.1 and 5.2.1) whereas the data from the same oceanographic setting published by Bruggmann et al. (2019) are more difficult to explain. Chromium concentrations change up to 4 nmol/kg or more between adjacent samples while other parameters, which show much larger dynamic ranges than Cr throughout the global ocean, are similar, suggesting no major change in water mass or major biogeochemical differences. Assessing the large-scale consistency of our data and those of Bruggmann et al. (2019) through a general comparison of all reported [Cr] data from the Pacific Ocean clearly reveals that our [Cr] results overlap with the previously established range, which is consistent among more than 40 years of oceanographic Cr research, and highlights that the concentrations reported by Bruggmann et al. (2019) are unusually high (supplemental Fig. S1).

Sediment Dynamics: A local sediment source is invoked to explain the elevated [Cr] reported by Bruggmann et al. (2019). However, observed surface ocean Cr enrichments

require large-scale vertical transport of dissolved Cr from sediments to the surface, which appears to be inconsistent with relatively low [Cr] at intermediate depths. Although the Peruvian coastal upwelling is a very dynamic region, mass balance considerations also demonstrate that it is difficult to explain the enrichments observed by Bruggmann et al. (2019) in the upper 900 m of the water column relative to our data based on episodic localized fluxes from sediments. We calculate that approximately 18% of sedimentary Cr would need to be released to the water column to explain the observed excess, which extends ~100 km offshore (see supplementary material). Given that most of the Cr in these sediments is in unreactive phases (Bruggmann et al., 2019), the necessary flux from sediments appears too large to be realistic, and an input from only a 250 km wide section of shelf would be comparable to the lower range of the total annual global Cr sources to the oceans (8×10^7 mol yr^{-1}, Bonnand et al., 2013). As reducing sediments are believed to be a net sink of Cr from the global ocean (Murray et al., 1983; Moos et al., 2020) it seems unlikely that such a small section of shelf is also a site of episodic Cr release of comparable magnitude to global marine Cr inputs.

In summary, considering the different methodologies, principles of oceanographic consistency, available regional and basin-scale data, and mass balance calculations, we are doubtful that the data of Bruggmann et al. (2019) reflect real oceanographic variability and thus refrain from incorporating these data into our discussions and interpretations. A more detailed description of these points is provided as supplementary information.

5.1. Biological control of marine Cr distribution and isotope composition

5.1.1. Surface depletion and regeneration at depth

Chromium concentrations [Cr] often feature moderate depletion at the surface and relative enrichment at depth, resembling nutrient-type depth profiles (Campbell and Yeats, 1981; Jeandel and Minster, 1987; Sirinawin et al., 2000; Scheiderich et al., 2015), and are often correlated with major nutrients (Cranston and Murray, 1978; Campbell and Yeats, 1981; Cranston, 1983). This observation has been attributed to biological uptake in the euphotic zone followed by regeneration from sinking particles in the deeper water column, with the continuous drawdown of surface water Cr into abyssal waters resulting in a concentration increase from the deep Atlantic to the deep Pacific Ocean (e.g. Jeandel and Minster, 1987; Connelly et al., 2006). More specifically, Cr(VI) is thought to be reduced to Cr(III) through either biology-mediated reduction or due to photochemical reactions in the surface ocean (e.g. Kieber and Helz, 1992; Connelly et al., 2006; Li et al., 2009), particularly in high productivity waters (Janssen et al., 2020) and shuttled down adsorbed to sinking phytoplankton cells (Semeniuk et al., 2016). Offshore stations 2, 28, 103 and 109 show [Cr] depth distributions consistent with these observations, as well as an inverse depth distribution of δ^{53}Cr that principally agrees with reductive removal of isotopically light Cr(III) from the euphotic zone and its transfer to the deep ocean. Deep water [Cr] offshore Peru range from 4.6 to 5.5 nmol/kg (depth > 1000 m) and thus exceed concentrations found in North Atlantic Deep Water (3550–5740 m; 2.5–2.8 nmol/kg; Goring-Harford et al., 2018), supporting the notion of increasing deep water Cr content along thermohaline circulation, while the range is similar to data from the deep northeastern Pacific (3000–4500 m; 4.5–4.8 nmol/kg; Moos and Boyle, 2019).

5.1.2. Diatoms as a vector for Cr transfer

Previous studies found [Cr] to be strongly correlated with $Si(OH)_4$, particularly in deeper waters (Campbell and Yeats, 1981; Cranston, 1983; Jeandel and Minster, 1987). Likewise, [Cr], δ^{53}Cr and $Si(OH)_4$ are well correlated across the full depth range at the offshore stations presented here (Fig. 4a/b), although we have to admit a low availability of coupled Si, [Cr] and δ^{53}Cr data for stations 2 and 28 (see also table 1). Nevertheless, the correlation is robust and its slope translates to a ratio of 0.016 nmol Cr kg^{-1}/μmol Si $(OH)_4$ kg^{-1}, which is between ratios presented for North and South Pacific deep and intermediate waters (0.01–0.023 nmol Cr kg^{-1}/ μmol $Si(OH)_4$ kg^{-1}; Jeandel and Minster, 1987), but higher than the 0.0076 nmol Cr kg^{-1}/ μmol $Si(OH)_4$ kg^{-1} published for the Cascadia basin (Cranston, 1983). This correlation is not necessarily evidence for a direct relationship between Cr and biogenic silica, but primary productivity is dominated by diatoms in the Peruvian coastal upwelling region (Bruland et al., 2005; Abrantes et al., 2007; Franz et al., 2012), and elemental analyses of phytoplankton reveal very similar Cr/Si $(OH)_4$ ratios of around 0.022 nmol kg^{-1}/μmol kg^{-1} (Martin and Knauer, 1973). Chromium was not found in the frustules themselves, but in a HNO_3-digested fraction comprising organics and frustule-adsorbed elements (Martin and Knauer, 1973). Consistently, Semeniuk et al. (2016) report surface adsorption (and to a lesser degree internalization) of Cr(III) onto phytoplankton cells (mostly diatoms) possibly acting as an important removal vector for surface water Cr. Concentrations of dissolved silicic acid increase with depth (and towards the south) due to intense remineralization of particulate biogenic silica in the water column and within the sediments in the study area (Ehlert et al., 2012), possibly releasing adsorbed particle reactive Cr(III).

Conflicting with the previous notions is the very different depth distribution of [Cr] and δ^{53}Cr when approaching the continental slope (stations 22 and 812) and above the Peruvian shelf (stations 19, 41, 806, 807), given that biological activity was highest close to shore during sampling (Franz et al., 2012; Grasse et al., 2016). Here, [Cr] profiles depart from the nutrient-type behavior and follow a depth distribution consistent with the removal of dissolved Cr close to the seafloor (stations 41, 806 and 807). Associated shifts in δ^{53}Cr mostly agree with the preferential removal of isotopically light Cr(III) (e.g. Schauble et al., 2004; Døssing et al., 2011). When added to the Cr vs. Si plot (Fig. 4c), samples from the slope and shelf area cluster at the low-Si end of the line, with markedly lower [Cr] compared to equal-depth counterparts further offshore. Lower [Cr] in surface waters above the shelf are however principally in

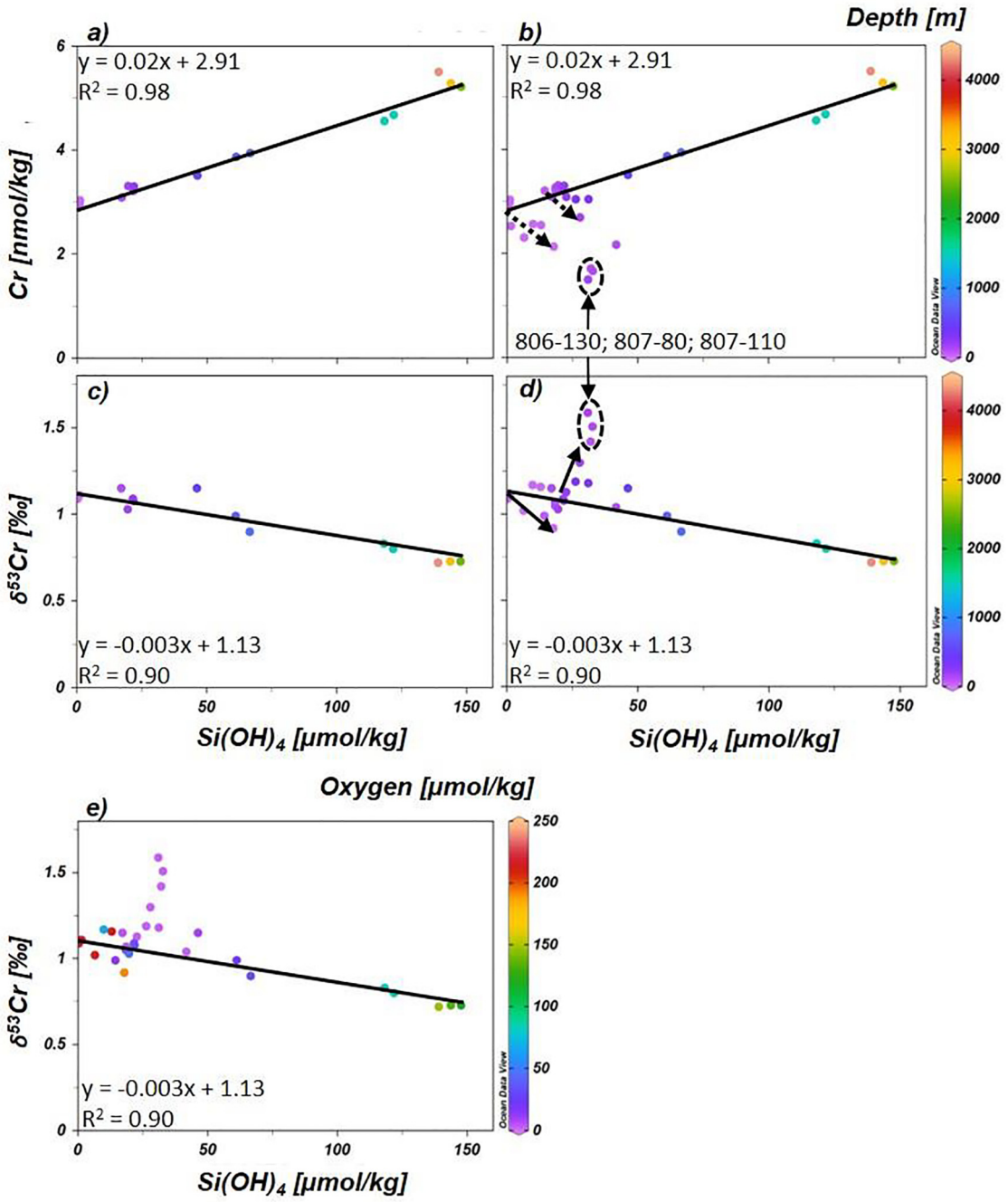

Fig. 4. Scatter plots with $Si(OH)_4$ vs. chromium concentrations (Cr or [Cr] in the main text) and isotopic compositions ($\delta^{53}Cr$) respectively. a/b) Displayed data are from offshore stations only. c/d) Data from offshore, slope and shelf stations (the regression is based solely on offshore stations). Indications of depth illustrate an apparently systematic offset of shelf samples compared to the offshore regression (stippled arrows), but differently evolving isotopic compositions (solid arrows). Samples 806–130, 807–80 and 807–110 seem to behave differently by showing stronger [Cr] depletion and the most extreme isotopic compositions. e) Same plot as (d) but with indication of oxygen levels instead of depth. Accordingly, the two different trends in evolution of $\delta^{53}Cr$ also agree with differences in oxygenation (highly oxygenated surface vs. OMZ waters).

agreement with higher biological activity and hence Cr removal. The offset from the Cr-$Si(OH)_4$ correlation line appears mostly systematic, lowering [Cr] while increasing [Si] at a fixed ratio (Fig. 4c), whereas samples from stations 806 (130 m) and 807 (80 and 110 m) show a stronger Cr depletion for the given Si-enrichment in the subsurface.

The relationship between Si and $\delta^{53}Cr$ is non-uniform and shows opposing directions. Although all samples are lower in [Cr] and enriched in Si, some evolve towards slightly lighter $\delta^{53}Cr$ (e.g. samples 19–0; 806–0; 812–50) or increasingly heavy $\delta^{53}Cr$ (e.g. samples 19–100; 806–130; 807–110) (Fig. 4d). The former $\delta^{53}Cr$ trend appears to

rather represent highly oxygenated surface and upper-water column samples that are influenced by upwelling of cold, nutrient-rich subsurface waters. Here, the high [Si] results from continuous re-supply of silica to the surface water pool, balancing utilization by diatoms more completely than further offshore (also reflected in heavy δ^{30}Si), but also stimulating higher primary productivity (Ehlert et al., 2012) that would draw down more particle-adsorbed Cr. On the contrary, samples from strongly oxygen-depleted waters ($O_2 < 5$ µmol/kg) between 80 m and 300 m depth evolve towards heavy δ^{53}Cr as [Cr] decreases (Fig. 4e), suggesting that different processes are at work. Here the high [Si] appears to stem from benthic fluxes (as reflected by light δ^{30}Si; Grasse et al., 2016; Ehlert et al., 2016) and Cr removal may be related to redox cycling.

5.2. Redox control on marine Cr distribution and isotope composition

5.2.1. Cr variability across oxygen concentration gradients

A redox control on Cr speciation and thus isotopic composition is the fundamental assumption behind the use of Cr isotopes as a paleo-redox proxy. Indeed, Cr(III) becomes the thermodynamically favored species under extremely low oxygen conditions (<2 µmol/kg) and high levels of Cr(III) have been detected in OMZs (e.g. Rue et al., 1997), which has led to the proposal of OMZs as an environment where removal of isotopically light Cr from the dissolved phase may potentially occur (e.g. Scheiderich et al., 2015). However, so far, no systematic variations of either [Cr] or δ^{53}Cr with changing dissolved oxygen concentration have been reported. Goring-Harford et al. (2018) investigated samples from the eastern equatorial Atlantic Ocean OMZ, offshore Senegal and found evidence supporting the removal of Cr from the water column above the shelf possibly resulting from high particle flux. No correlation with dissolved oxygen was observed at the prevailing conditions (dissolved oxygen ≥44 µmol/kg), which may not have been reducing enough to promote the reduction of Cr(VI).

The data presented here also show no systematic δ^{53}Cr variation across the full range of dissolved oxygen concentrations (<2–242 µmol/kg; Fig. 5a/b). Noticeably, high δ^{53}Cr values are found in both low oxygen and high oxygen environments. The latter, however, are exclusively associated with surface water samples (low densities $\sigma_\theta < 26$ kg/m^3, Fig. 5b) where Cr reduction may be achieved by biological processes or photochemistry. Ignoring surface waters, a trend towards lower [Cr] (Fig. 5a) and higher δ^{53}Cr values (Fig. 5b) with decreasing oxygen concentrations

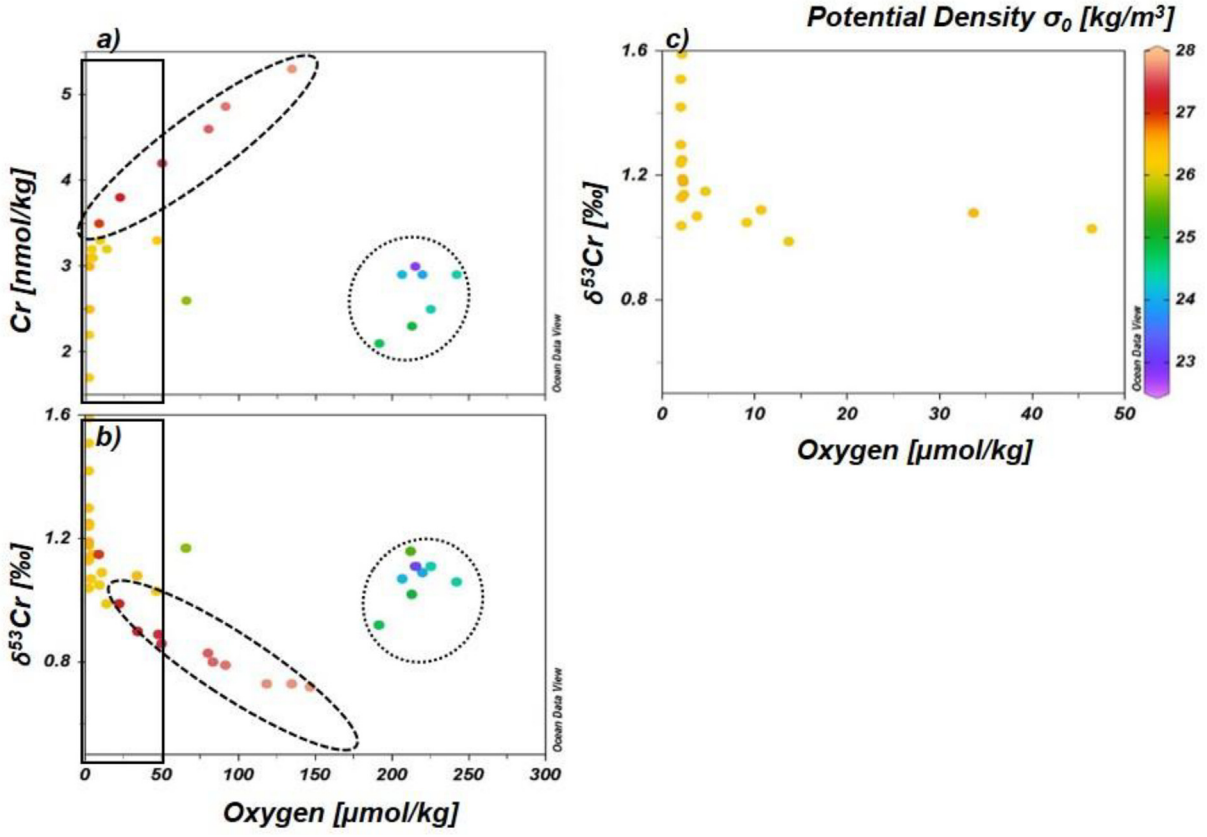

Fig. 5. a) Chromium concentrations (Cr or [Cr] in the main text) and isotope data (δ^{53}Cr) in relation to dissolved oxygen concentrations and potential density (σ_θ) for all samples (b). c) The highly fractionated samples from the most oxygen-depleted (<50 µmol/kg) areas and the $\sigma_\theta = 26$ kg/m3 (Equatorial Subsurface Water) density surface (black frame in 5a/b). Surface (depth ≤ 10 m; dotted line) and deep waters (depth ≥ 500 m; stippled line) are highlighted additionally.

becomes apparent, affecting all water masses below the oxycline. The trend is relatively linear between ~10 and ~130 μmol/kg O_2 and also a function of potential density (σ_θ) thus possibly representing mixing of different water masses below 500 m. For oxygen concentrations <10 μmol/kg, however, [Cr] and δ^{53}Cr vary widely, with concentrations ranging from 1.5 to 3.5 nmol/kg and δ^{53}Cr from ~+1 to +1.6‰. These low-oxygen waters are almost exclusively attributed to Equatorial Subsurface Water ($\sigma_\theta = 26$ kg/m^3), the water carried by the PCUC (e.g. Fiedler and Talley, 2006) so that the observed [Cr] and δ^{53}Cr variability is clearly not a consequence of water mass mixing. Fig. 5c shows the [O_2] - δ^{53}Cr relationship for this water mass and suggests that Cr isotope shifts occur only below a threshold value of ~5 μmol/kg of dissolved oxygen. Since most shifts towards heavier δ^{53}Cr are associated with lowered [Cr] (only exceptions are samples 2–100 and 22–150), Cr input from an isotopically heavy pool (such as shelf sediments; Goring-Harford et al., 2018) is not supported by our data for the Peruvian OMZ. Instead, reductive removal appears to be the most likely mechanism to produce the observed pattern, although no Cr speciation data is available to substantiate that Cr reduction indeed occurs.

5.2.2. Cr variability linked to denitrification?

Even though Cr reduction appears to occur under suboxic conditions ([O_2] < 5 μmol/kg), it remains unclear whether this is general thermodynamic response or whether a specific, non-ubiquitous reducing agent is required to facilitate the transition. Suboxic conditions also exist within the offshore OMZ (though limited to a much smaller depth range), but observations of Cr reduction, as inferred from [Cr] and δ^{53}Cr covariation, are confined to shelf waters. The spatial confinement may hint towards requirement of a reducing agent that is not widely available.

Some studies suggest an association of Cr cycling with the nitrogen cycle as peaks in Cr(III), or lower total [Cr] concentrations and thus heavier δ^{53}Cr often correlate with a nitrite maximum (Cranston and Murray, 1978; Moos et al., 2020). Indeed, samples from sub- to anoxic waters of this study behave similarly, and there is a strong correlation between the two nitrogen species (nitrate/nitrite), [Cr] and δ^{53}Cr (Fig. 6), whereby [Cr] decreases and δ^{53}Cr increases as more nitrite accumulates. This could indicate a link between Cr reduction and microbial denitrification (Moos et al., 2020), possibly in conjunction with (nitrate-dependent) oxidation of Fe(II) to Fe-oxyhydroxides (e.g. Scholz et al., 2014) providing a scavenging surface to remove reduced Cr(III) from the dissolved phase (Goring-Harford et al., 2018). However, the presence of appreciable nitrite and evidence for nitrate reduction are key features of suboxic waters with O_2 < 5 μmol/kg (Brandhorst, 1958; Rue et al., 1997). Furthermore, the similar redox potentials for Cr(VI) and nitrate (Bratsch, 1989; Fanning, 2000) suggest environmental conditions facilitating reduction of nitrate should also enable reduction of Cr(VI) without necessarily requiring a relationship between the two. Nevertheless, it could be promising to dedicate future research to unravel a potential link between microbial denitrification and Cr reduction.

5.2.3. Reducing agents facilitating Cr reduction in OMZ waters

Amongst the several reducing agents available for reduction of Cr(VI), Fe(II) and H_2S are more commonly found in environments characterized by extreme oxygen depletion (Pettine, 2000). Anoxic bottom waters facilitate fluxes of sediment-released Fe(II) into the water column (e.g. Scholz et al., 2014) and sporadic sulfidic events allow for significant levels of H_2S in Peruvian shelf waters (e.g. Schunck et al., 2013).

Limited availability of dissolved Fe data does not allow for a thorough investigation of a potential relationship between Fe(II) and Cr reduction, but we would like to emphasize some parallel occurrences. Schlosser and coworkers measured dissolved Fe concentrations at stations 807 (2–30 nmol/kg, referred to as site #1, Schlosser et al., 2018), 19 (80–267 nmol/kg, referred to as site #2; Schlosser et al., 2018) and 28 (1.2–5.2 nmol/kg measured within the upper 800 m, Schlosser and Croot, 2019) and suggested that these concentrations should likely represent Fe(II), although this is only backed by Fe-speciation measurements at station 19. While stations 807 and 28 show highest Fe concentrations at depths of apparent Cr reduction, no such co-occurrence is evident at station 19, despite the exceptional Fe(II) level and a large dissolved H_2S plume (up to 4 μmol/kg) at the time of sampling (Schlosser et al., 2018).

Why significant evidence for reductive Cr removal is missing in the most reducing setting encountered in this study remains unclear. Certainly, the Cr water column profile is incomplete and we can only speculate about the apparent lack of Cr removal: 1) Stabilized as aqueous Fe-sulfide complexes (Schlosser et al., 2018), Fe(II) may not be able to reduce Cr(VI). 2) Sulfide-mediated Cr(VI) reduction may proceed only slowly (Pettine et al., 1994), perhaps too slow considering the transient nature of sulfidic events (e.g. Schlosser et al., 2018). 3) Cr(VI) may get reduced, but not removed, since removal of Cr is also controlled by the availability of particulate surfaces and not by reduction alone. Previous work has demonstrated that Cr(III) can stay in solution (e.g. Connelly et al., 2006; Saad et al., 2017). In this context it is interesting to note that the two data points from station 19 plot clearly below the global trend line (Fig. 3).

5.3. Chromium isotope fractionation models

In the previous sections we collected information that supports different controls on Cr distribution and isotopic composition within the different environments of coastal Peru. While offshore stations principally agree with biologically mediated Cr reduction within the euphotic zone and depth transfer of Cr(III), the highly variable [Cr] and δ^{53}Cr observed above the shelf suggest different controls on Cr distribution in oxygenated surface waters and suboxic/anoxic water column below.

Upwelling of PCUC waters suggests that surface waters are in a state of dynamic equilibrium, where partial depletion of the Cr pool due to biologically mediated removal is balanced by continuous supply from the subsurface.

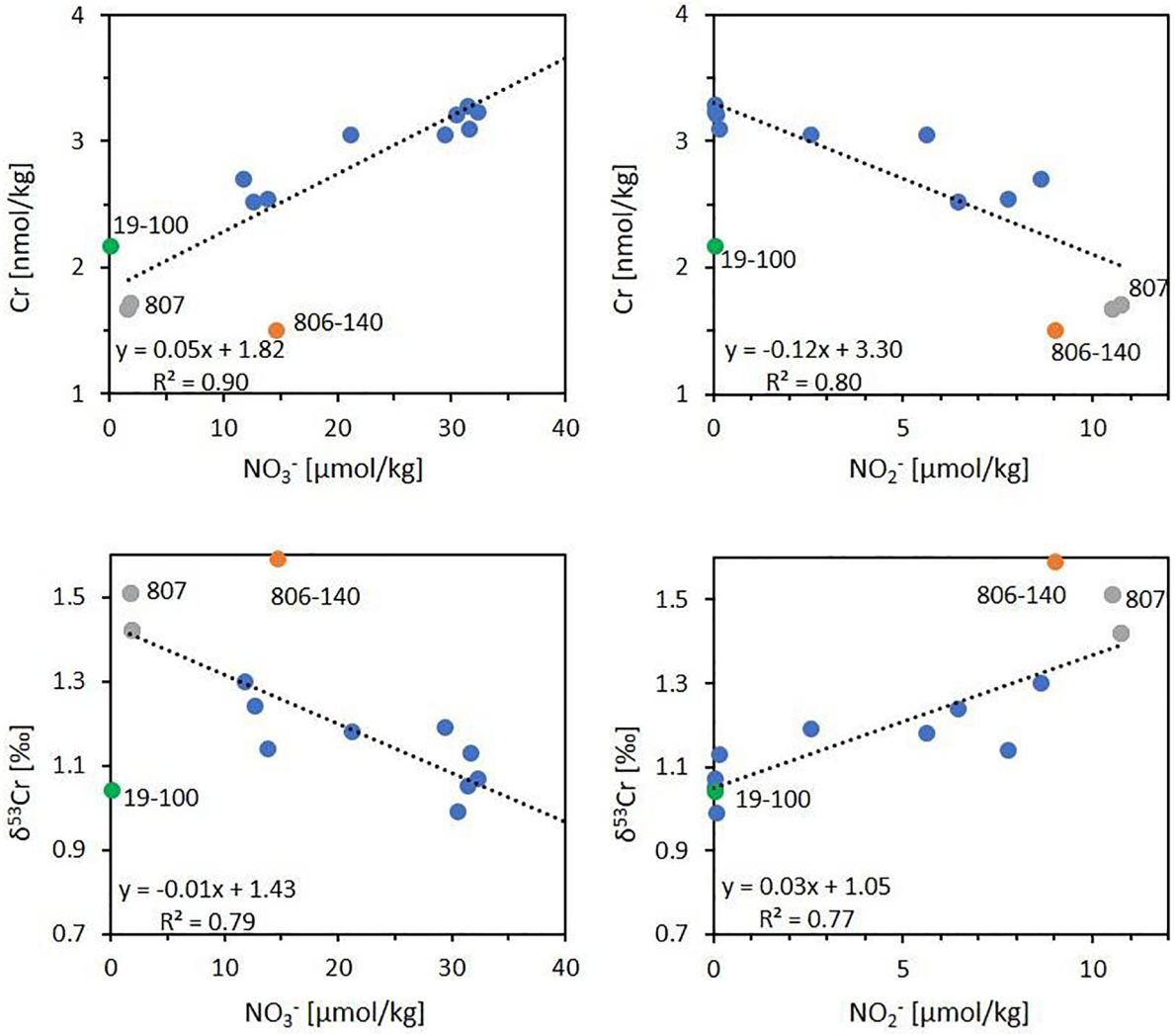

Fig. 6. Chromium concentration and isotope composition versus nitrate and nitrite for all shelf and slope samples with dissolved oxygen < 50 µmol/kg (blue dots). Samples indicating Cr reduction (as inferred from [Cr] and δ 53Cr covariation) or dissolved Cr(III) (station 19; see also main text) are highlighted in different colors. Out of these, only samples from station 807 are included into the regression. Samples 19–100 and 807–80 also feature high dissolved Fe(II) (188 nM and 30 nM respectively, Schlosser et al., 2018), whereas no Fe data were available for sample 807–110. (For interpretation of the references to colour in this figure legend, the reader is referred to the web version of this article.)

However, previous publications suggested alterations of the biogeochemical properties of the PCUC during southward transport due to enhanced remineralization within the OMZ and processes at the seawater-sediment boundary (Bruland et al., 2005) and hence the source signature of the upwelled water may vary from station to station. According to literature, PCUC waters are sourced between 50 and 150 m (Ehlert et al., 2012; Grasse et al., 2016) and samples from within this depth range indeed show large variability. Some of the bottom waters show significant Cr depletion that is more reminiscent of a Rayleigh-type model, describing a system in which after a single input no additional Cr is supplied to the system:

$$\delta^{53}Cr_{\ Observed} = \delta^{53}Cr_{\ Init} - \varepsilon * (\ln f)$$
$$\delta^{53}Cr_{\ Inst\ Removed} = \delta^{53}Cr_{\ Observed} + \varepsilon$$
$$\delta^{53}Cr_{\ Accum\ Removed} = \delta^{53}Cr_{\ Init} - \varepsilon^{*}(f \ln f / 1 - f)$$

where $\delta^{53}Cr_{\ Init}$ is the dissolved Cr isotope composition of the system before Cr is gradually removed to particles, $\delta^{53}Cr_{\ Observed}$ reflects the evolution of the dissolved pool as removal proceeds, $\delta^{53}Cr_{\ Inst\ Removed}$ represents the isotopic composition of the instantaneously produced particle reactive Cr(III) for a given f and $\delta^{53}Cr_{\ Accum\ Removed}$ integrates the fractionation over time in the accumulated Cr (III) pool. The fraction f describes the fraction of the dissolved initial [Cr] that remains and ε is the isotope fractionation factor. (We note that some of the reduced particle reactive Cr(III) may remain in solution and contribute to the $\delta^{53}Cr_{\ Observed}$, see Section 5.2.3 and below).

The initial composition of the PCUC is difficult to approximate. Grasse et al. (2016) used the water composi-

tion from 50 to 140 m at station 806 as a representative for the silicon composition of PCUC waters. However, the two depths sampled for Cr within this depth range (at 81 and 141 m; Table 1) are very different and preclude robustly identifying an endmember under this criterion. In fact, station 806 is the prime example of redox-dependent modification of Cr and displays a clear change in [Cr] and δ^{53}Cr under suboxic conditions (Fig. 2a). The 80 meters depth sample (806–80) comes from above the suboxic zone and may provide a close approximation of unmodified PCUC water at this station. Comparison with offshore samples from similar density surfaces (summarized in Table 2) reveals similar [Cr] and δ^{53}Cr, supporting 806–80 as an initial PCUC endmember within our dataset.

Fig. 7a shows a Rayleigh fractionation model (black stippled and solid lines) utilizing sample 806–80 as source composition ($[Cr]_{Init}$ and $\delta^{53}Cr_{Init}$) and $\varepsilon = -0.8‰$, the apparent fractionation factor governing the Cr isotopic composition of the global open ocean (e.g. Scheiderich et al., 2015; Goring-Harford et al., 2018; Rickli et al., 2019) along with measured δ^{53}Cr from subsurface shelf samples (blue dots). Most samples follow the Rayleigh model well, although a smaller fractionation factor in the range between −0.6 and −0.7‰ would provide a better overall fit. Even samples from station 41 (unfilled dots), which were collected at latitudes where this depth range includes a mixture of PCUC and PCCC rather than pure PCUC (e.g. Czeschel et al., 2011; Ehlert et al., 2012) agree with the model. As shown by this model, PCUC waters experience modification above the shelf during alongshore transport. Accordingly, as the presented model highlights the variability of the subsurface waters, this precludes any modelling of the surface waters due to changes to the PCUC upwelling signature during along-shelf flow.

Table 2
Comparison of samples from offshore stations and the northern shelf to constrain the composition of water carried by the PCUC (all data also presented in Table 1).

Station	Depth [m]	Temperature [°C]	Salinity [PSU]	Oxygen [µmol/kg]	Potential Density [kg/m^3]	NO_3^- [µmol/kg]	[Cr] [nmol/kg]	δ^{53}Cr [‰]	2SE [‰]
103	151	13.06	34.95	10.7	26.35	30.89	3.22	1.09	0.02
109	151	13.53	34.96	46.4	26.27	27.64	3.31	1.03	0.03
806	81	14.08	34.99	9.1	26.17	31.49	3.28	1.05	0.04
806	141	13.74	34.97	2.1	26.23	14.71	1.50	1.59	0.03

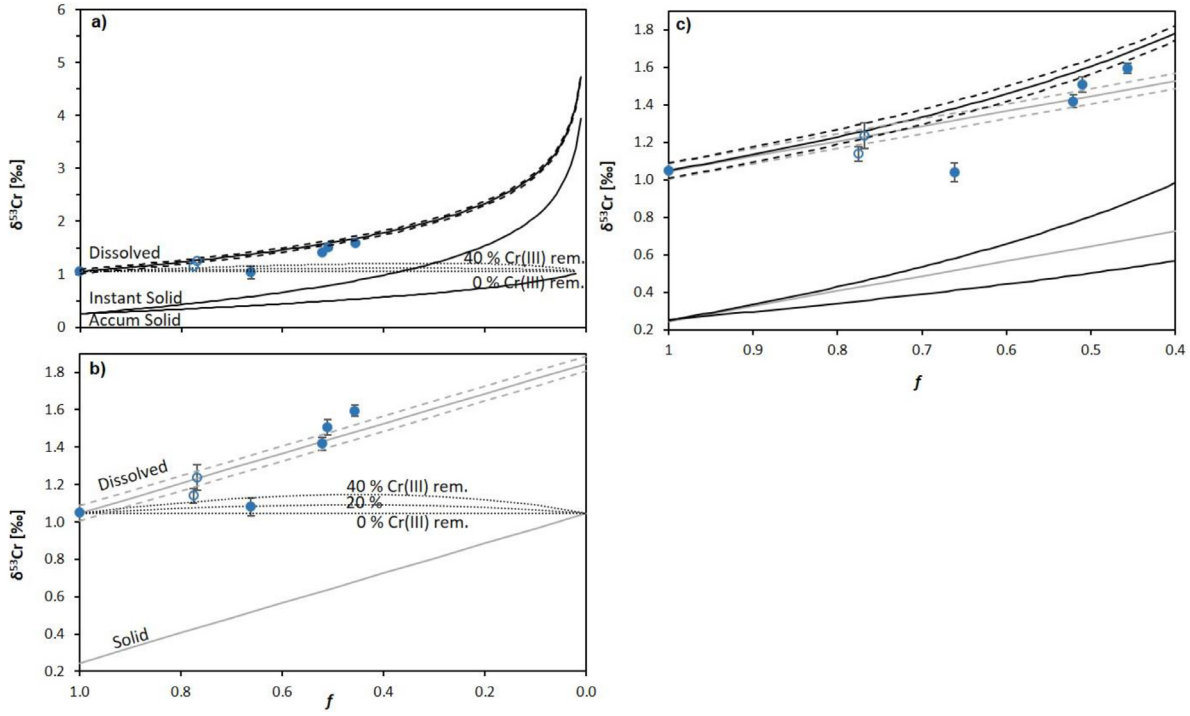

Fig. 7. Rayleigh-type (a) and steady-state (b) isotope fractionation models for $\varepsilon = -0.8‰$. Fractionation lines representing the evolution of δ^{53}Cr for dissolved Cr(VI) (with uncertainty brackets, stippled lines) and solid phase Cr(III), as well as the instantaneously forming solid (only in (a)) are displayed in all plots. Moreover, model scenarios simulating only partial removal (0, 20, 40%) of reduced Cr(III) to the solid phase are included in a) and b). c) Combined plot of Rayleigh (black) and steady-state (grey) models for $f > 0.4$. Included in all plots are measured δ^{53}Cr from shelf samples within the PCUC depth range (blue dots) and from station 41 (unfilled circles), although these were collected at latitudes where this depth range includes a mixture of PCUC and PCCC rather than pure PCUC (see main text for more information). (For interpretation of the references to colour in this figure legend, the reader is referred to the web version of this article.)

For completeness, we also present a steady-state model with the same $[Cr]_{Init}$ and $\delta^{53}Cr_{Init}$ and ε (Fig. 7b; grey stippled and solid lines). Included are measured $\delta^{53}Cr$ from shelf samples within the PCUC depth range (blue dots), which broadly also agree with this model. Here, a slightly higher fractionation factor around −0.9‰ would provide a better overall fit. A direct comparison of the Rayleigh and the steady-state model (Fig. 7c) suggests that as more Cr(III) is removed (towards $f < 0.5$) and residual Cr(VI) evolves towards heavier $\delta^{53}Cr$, the Rayleigh model may predict the trend of $\delta^{53}Cr$ more accurately.

These modeled data are based on isotope analysis of total Cr as opposed to species-specific isotope analyses of Cr(VI) and Cr(III). Therefore, due to the large fractionations associated with Cr reduction (e.g. Ellis et al., 2002; Døssing et al., 2011), models typically rely on the assumption that the dissolved Cr pool is dominated by Cr(VI), and that any Cr(III) produced through reduction adsorbs immediately to particles and is removed from the dissolved phase. However, this assumption may be incorrect in certain environments. Several studies have reported significantly higher dissolved Cr(III) fractions than predicted by thermodynamic principles (e.g. Murray et al., 1983; Jeandel and Minster, 1987; Achterberg and van den Berg, 1997; Connelly et al., 2006) and others have demonstrated that organic complexation is capable of keeping Cr(III) in solution (e.g. Saad et al., 2017). Due to the very slow oxidation kinetics of Cr (Scheiderich et al., 2015 and references therein), Cr(III) liberated from decomposed particles may even persist without organic complexation in OMZ waters and accumulate. The consequences for measured total dissolved $\delta^{53}Cr$ containing Cr(VI) and Cr(III) would involve an attenuated apparent isotope fractionation reflecting the net effect of reduction and scavenging processes as well as possible isotope effects upon organic complexation. Modelled fractionation lines with $\varepsilon = -0.8‰$ but assuming that 100, 80, or 60% of Cr(III) remain dissolved (respectively, removal of only 0, 20, or 40% of Cr(III)) are drawn in Fig. 7a & b (dotted lines). These models demonstrate that the $\delta^{53}Cr$ of sample 19–97 could be attributed to such a scenario. Data are not available to verify these concepts for our samples; however, because Cr(III) becomes more relavant in suboxic waters (Rue et al., 1997), the presence of both Cr species in the dissolved phase should be considered in future studies of these environments and also when compiling global data in general.

Summarizing the findings from this model approach, our data suggest that the PCUC loses Cr due to redox-controlled processes and that this Cr is removed to anoxic marine sediments on the shelf, which have long been suggested as the main Cr sink (Jeandel and Minster, 1987). In agreement with the presented Rayleigh and steady-state models, this would preferentially remove isotopically light Cr and drive the residual dissolved Cr towards heavier $\delta^{53}Cr$. This low [Cr], heavy $\delta^{53}Cr$ water may get upwelled to the surface, thereby creating a smooth transition through mixing, such as observed at station 807. Alternatively, isotopically light Cr(III) released upon decomposition of sinking phytoplankton cells at intermediate depth could explain the more abrupt transition observed at station 806. Unfortunately, the observed modification of the PCUC along its flow path parallel to the Peruvian Coast, and within each "upwelling cell" fed by the PCUC, together with southward transport of subsurface waters and northward transport of surface waters above the shelf, preclude any meaningful modelling of surface processes.

6. CONCLUSIONS

Dissolved seawater Cr concentrations and stable isotope compositions were investigated along depth profiles across the Peru margin OMZ, covering a wide spectrum of dissolved oxygen concentrations and biogeochemically distinct settings. Although there is no single relationship between dissolved oxygen concentrations and Cr dynamics across the shelf, slope and open ocean settings, our data imply that large-scale Cr reduction and removal in OMZs requires suboxic conditions and occurs primarily in shelf settings. We do not find evidence of shelf sediments acting as a major Cr source. Removal of Cr from the dissolved pool on the shelf, associated with enrichments of isotopically heavy Cr in the residual dissolved phase, suggests reduction of Cr(VI) to Cr(III) and is best approximated by a Rayleigh-type fractionation model, with some observations suggesting only partial removal of the reduced Cr(III) to the particulate phase. The fundamental responsible mechanisms remain poorly constrained at this stage. Spatial confinement of Cr reduction and removal to the shelf and coinciding anomalies in nitrate and nitrite concentrations may hint towards a link to denitrification, but specific reducing agents in the water column may also be involved as electron donor. In contrast to shelf sites, offshore stations feature nutrient type [Cr] depth profiles consistent with biologically mediated Cr reduction in the euphotic zone and regeneration at depth, although the deep waters are likely dominated by preformed [Cr] and $\delta^{53}Cr$. The open ocean deep waters and anoxic shelf waters thus represent the two environmental extremes in Cr concentrations and $\delta^{53}Cr$ in the study area. Whether the different processes amount to different fractionation factors is difficult to deduce from the presented data set, since all derived fractionation factors (∼−0.6 to −0.7‰ from the Rayleigh model and ∼−0.9‰ from the steady state model -both Section 5.3- as well as $-0.7 \pm 0.08‰$ from the global trend line; Fig. 3) represent the net effect of reduction, scavenging and possibly other processes.

The global impact of Cr removal in suboxic/anoxic shelf waters is difficult to assess. So far, this mechanism was only observed at few locations above the Peruvian shelf between 3° and 17°S, and only in suboxic waters (this study). The suboxic/anoxic shelf area offshore Peru covers roughly 68,000 km^2 (Helly and Levin, 2004), which is negligible compared to the global ocean surface area. On the contrary, Cr removal above the Peruvian shelf appears to be efficient and some samples imply a Cr deficit of ∼50% compared to the initial PCUC composition (see Section 5.3; Fig. 7), lost within a fraction of the entire shelf length. Hence, with sluggish circulation, substantial Cr loss from a given water mass may occur while transiting suboxic shelf areas. Whether the strength of this removal mechanism var-

ies over time is not known, but it is conceivable that the dynamic conditions in the Peruvian upwelling area also facilitate fluctuations in Cr removal. Globally, suboxic shelf areas cover a much wider surface than the Peruvian shelf alone and if Cr removal were detected there as well it could become a significant process within the global marine Cr cycle. More data are required to substantiate and quantify redox- as well as biologically-mediated Cr removal and comparability between studies and labs needs improvement through an intercalibration effort. Moreover, future research should more thoroughly investigate the fundamental mechanisms behind Cr removal in suboxic waters and potential links to microbial denitrification and/or sediment-derived Fe(II). Suboxic Cr removal may differ from oxic removal-mechanisms related to biological activity in the euphotic zone, which are also poorly constrained at present. Finally, a better understanding of the role and abundance of dissolved Cr(III) is desirable as isotope fractionation models and also the global correlation in δ^{53}Cr-ln ([Cr]) space are biased towards the concept of dissolved Cr (VI) vs. particle-adsorbed Cr(III).

Data availability statement

Research Data associated with this article can be accessed at https://doi.org/10.5281/zenodo.3630186.

Declaration of Competing Interest

The authors declare that they have no known competing financial interests or personal relationships that could have appeared to influence the work reported in this paper.

ACKNOWLEDGEMENTS

Cruise M77 and SFB 754 – *Sonderforschungsbereich 754 "Climate - Biogeochemistry Interactions in the Tropical Ocean*" - during which the sampling was carried out, were funded by the German Research Foundation (DFG). Funding for PN was provided by the German Research Foundation (DFG) through a postdoctoral research fellowship (project number 395901092). This project has received funding from the Swiss National Science Foundation (grant PP00P2_172915) and the European Research Council (ERC) under the European Union's Horizon 2020 research and innovation programme (Grant agreement No. 819139 – SCrIPT). Chromium data were obtained on a Neptune MC-ICP-MS acquired with funds from the NCCR PlanetS supported by SNSF grant 51NF40-141881 (Economou-Eliopoulos et al., 2016).

APPENDIX A. SUPPLEMENTARY MATERIAL

Supplementary data to this article can be found online at https://doi.org/10.1016/j.gca.2020.06.027.

REFERENCES

Abrantes F., Lopes C., Mix A. and Pisias N. (2007) Diatoms in Southeast Pacific surface sediments reflect environmental properties. *Quat. Sci. Rev.* **26**, 155–169.

Achterberg E. P. and van den Berg C. M. G. (1997) Chemical speciation of chromium and nickel in the western Mediterranean. *Deep Sea Res Part II Top. Stud. Oceanogr.* **44**, 693–720.

Ball J. W. and Bassett R. L. (2000) Ion exchange separation of chromium from natural water matrix for stable isotope mass spectrometric analysis. *Chem. Geol.* **168**, 123–134.

Bonnand P., James R. H., Parkinson I. J., Connelly D. P. and Fairchild I. J. (2013) The chromium isotopic composition of seawater and marine carbonates. *Earth Planet. Sci. Lett.* **382**, 10–20.

Boyle E. A., Sclater F. R. and Edmond J. M. (1977) The distribution of dissolved copper in the Pacific. *Earth Planet. Sci. Lett.* **37**, 38–54.

Brandhorst W. (1958) Nitrite accumulation in the north-east tropical pacific. *Nature* **182**, 679.

Bratsch S. G. (1989) Standard electrode potentials and temperature coefficients in water at 298.15 K. *J. Phys. Chem. Ref. Data* **18**, 1–21.

Brink K. H., Halpern D., Huyer A. and Smith R. L. (1983) The physical environment of the Peruvian upwelling system. *Prog. Oceanogr.* **12**, 285–305.

Bruggmann S., Scholz F., Klaebe R. M., Canfield D. E. and Frei R. (2019) Chromium isotope cycling in the water column and sediments of the Peruvian continental margin. *Geochim. Cosmochim. Acta* **257**, 224–242.

Bruland K. W., Rue E. L., Smith G. J. and DiTullio G. R. (2005) Iron, macronutrients and diatom blooms in the Peru upwelling regime: brown and blue waters of Peru. *Mar. Chem.* **93**, 81–103.

Campbell J. A. and Yeats P. A. (1981) Dissolved chromium in the northwest Atlantic Ocean. *Earth Planet. Sci. Lett.* **53**, 427–433.

Canfield D. E., Zhang S., Frank A. B., Wang X., Wang H., Su J., Ye Y. and Frei R. (2018) Highly fractionated chromium isotopes in Mesoproterozoic-aged shales and atmospheric oxygen. *Nat. Commun.* **9**, 2871.

Cole D. B., Reinhard C. T., Wang X., Gueguen B., Halverson G. P., Gibson T., Hodgskiss M. S. W., McKenzie N. R., Lyons T. W. and Planavsky N. J. (2016) A shale-hosted Cr isotope record of low atmospheric oxygen during the Proterozoic. *Geology* **44**, 555–558.

Connelly D. P., Statham P. J. and Knap A. H. (2006) Seasonal changes in speciation of dissolved chromium in the surface Sargasso Sea. *Deep Sea Res. Part I Oceanogr. Res. Pap.* **53**, 1975–1988.

Cranston R. E. (1983) Chromium in Cascadia Basin, northeast Pacific Ocean. *Mar. Chem.* **13**, 109–125.

Cranston R. E. and Murray J. W. (1978) The determination of chromium species in natural waters. *Anal. Chim. Acta* **99**, 275–282.

Crowe S. A., Døssing L. N., Beukes N. J., Bau M., Kruger S. J., Frei R. and Canfield D. E. (2013) Atmospheric oxygenation three billion years ago. *Nature* **501**, 535.

Czeschel R., Stramma L., Schwarzkopf F. U., Giese B. S., Funk A. and Karstensen J. (2011) Middepth circulation of the eastern tropical South Pacific and its link to the oxygen minimum zone. *J. Geophys. Res. Ocean.*, 116.

Davidson A. B., Semeniuk D. M., Koh J., Holmden C., Jaccard S. L., Francois R. and Crowe S. A. (2020) A Mg(OH)2 coprecipitation method for determining chromium speciation and isotopic composition in seawater. *Limnol. Oceanogr. Methods* **18**, 8–19.

Døssing L. N., Dideriksen K., Stipp S. L. S. and Frei R. (2011) Reduction of hexavalent chromium by ferrous iron: a process of chromium isotope fractionation and its relevance to natural environments. *Chem. Geol.* **285**, 157–166.

Economou-Eliopoulos M., Frei R. and Megremi I. (2016) Potential leaching of Cr(VI) from laterite mines and residues of metal-

lurgical products (red mud and slag): an integrated approach. *J. Geochem. Explor.* **162**, 40–49.
Ehlert C., Doering K., Wallmann K., Scholz F., Sommer S., Grasse P., Geilert S. and Frank M. (2016) Stable silicon isotope signatures of marine pore waters – Biogenic opal dissolution versus authigenic clay mineral formation. *Geochim. Cosmochim. Acta* **191**, 102–117.
Ehlert C., Grasse P., Mollier-Vogel E., Böschen T., Franz J., de Souza G. F., Reynolds B. C., Stramma L. and Frank M. (2012) Factors controlling the silicon isotope distribution in waters and surface sediments of the Peruvian coastal upwelling. *Geochim. Cosmochim. Acta* **99**, 128–145.
Elderfield H. (1970) Chromium speciation in sea water. *Earth Planet. Sci. Lett.* **9**, 10–16.
Ellis A. S., Johnson T. M. and Bullen T. D. (2002) Chromium isotopes and the fate of hexavalent chromium in the environment. *Science* **295**, 2060–2062.
Fanning J. C. (2000) The chemical reduction of nitrate in aqueous solution. *Coord. Chem. Rev.* **199**, 159–179.
Farkaš J., Frýda J., Paulukat C., Hathorne E. C., Matoušková Š., Rohovec J., Frýdová B., Francová M. and Frei R. (2018) Chromium isotope fractionation between modern seawater and biogenic carbonates from the Great Barrier Reef, Australia: implications for the paleo-seawater δ53Cr reconstruction. *Earth Planet. Sci. Lett.* **498**, 140–151.
Fiedler P. C. and Talley L. D. (2006) Hydrography of the eastern tropical Pacific: a review. *Prog. Oceanogr.* **69**, 143–180.
Franz J., Krahmann G., Lavik G., Grasse P., Dittmar T. and Riebesell U. (2012) Dynamics and stoichiometry of nutrients and phytoplankton in waters influenced by the oxygen minimum zone in the eastern tropical Pacific. *Deep Sea Res. Part I Oceanogr. Res. Pap.* **62**, 20–31.
Frei R., Gaucher C., Poulton S. W. and Canfield D. E. (2009) Fluctuations in Precambrian atmospheric oxygenation recorded by chromium isotopes. *Nature* **461**, 250–253.
Frei R., Paulukat C., Bruggmann S. and Klaebe R. M. (2018) A systematic look at chromium isotopes in modern shells – implications for paleo-environmental reconstructions. *Biogeosciences* **15**, 4905–4922.
Frei R., Poiré D. and Frei K. M. (2014) Weathering on land and transport of chromium to the ocean in a subtropical region (Misiones, NW Argentina): a chromium stable isotope perspective. *Chem. Geol.* **381**, 110–124.
Fuenzalida R., Schneider W., Garcés-Vargas J., Bravo L. and Lange C. (2009) Vertical and horizontal extension of the oxygen minimum zone in the eastern South Pacific Ocean. *Deep Sea Res. Part II Top. Stud. Oceanogr.* **56**, 992–1003.
Goring-Harford H. J., Klar J. K., Pearce C. R., Connelly D. P., Achterberg E. P. and James R. H. (2018) Behaviour of chromium isotopes in the eastern sub-tropical Atlantic Oxygen Minimum Zone. *Geochim. Cosmochim. Acta* **236**, 41–59.
Grasse P., Ryabenko E., Ehlert C., Altabet M. A. and Frank M. (2016) Silicon and nitrogen cycling in the upwelling area off Peru: a dual isotope approach. *Limnol. Oceanogr.* **61**, 1661–1676.
Helly J. J. and Levin L. A. (2004) Global distribution of naturally occurring marine hypoxia on continental margins. *Deep Sea Res. Part I Oceanogr. Res. Pap.* **51**, 1159–1168.
Holmden C., Jacobson A. D., Sageman B. B. and Hurtgen M. T. (2016) Response of the Cr isotope proxy to Cretaceous Ocean Anoxic Event 2 in a pelagic carbonate succession from the Western Interior Seaway. *Geochim. Cosmochim. Acta* **186**, 277–295.
Janssen D. J., Rickli J., Quay P. D., White A. E., Nasemann P. and Jaccard S. L. (2020) Biological control of chromium redox and stable isotope composition in the surface ocean. *Global Biogeochem. Cycles*.
Jeandel C. and Minster J.-F. (1984) Isotope dilution measurement of inorganic chromium(III) and total chromium in seawater. *Mar. Chem.* **14**, 347–364.
Jeandel C. and Minster J. F. (1987) Chromium behavior in the ocean: global versus regional processes. *Global Biogeochem. Cycles* **1**, 131–154.
Karstensen J., Stramma L. and Visbeck M. (2008) Oxygen minimum zones in the eastern tropical Atlantic and Pacific oceans. *Prog. Oceanogr.* **77**, 331–350.
Kieber R. J. and Helz G. R. (1992) Indirect photoreduction of aqueous chromium(VI). *Environ. Sci. Technol.* **26**, 307–312.
Larsen K. K., Wielandt D., Schiller M. and Bizzarro M. (2016) Chromatographic speciation of Cr(III)-species, inter-species equilibrium isotope fractionation and improved chemical purification strategies for high-precision isotope analysis. *J. Chromatogr. A* **1443**, 162–174.
Li S.-X., Zheng F.-Y., Hong H.-S., Deng N. and Lin L.-X. (2009) Influence of marine phytoplankton, transition metals and sunlight on the species distribution of chromium in surface seawater. *Mar. Environ. Res.* **67**, 199–206.
Martin J. H. and Knauer G. A. (1973) The elemental composition of plankton. *Geochim. Cosmochim. Acta* **37**, 1639–1653.
Mayer L. M. (1988) Geochemistry of chromium in the oceans. In: Nriagu, J.O., Nieboer, E. (Eds.), Chromium in the Natural and Human Environments. Wiley Ser. Adv. Environ. Sci. Technol. 20, 173–187.
Moos S. B. and Boyle E. A. (2019) Determination of accurate and precise chromium isotope ratios in seawater samples by MC-ICP-MS illustrated by analysis of SAFe Station in the North Pacific Ocean. *Chem. Geol.* **511**, 481–493.
Moos S. B., Boyle E. A., Altabet M. A. and Bourbonnais A. (2020) Investigating the cycling of chromium in the oxygen deficient waters of the Eastern Tropical North Pacific Ocean and the Santa Barbara Basin using stable isotopes. *Mar. Chem.* **221** 103756.
Murray J. W., Spell B. and Paul B. (1983) The Contrasting geochemistry of manganese and chromium in the eastern tropical pacific ocean. In *Trace Metals in Sea Water* (eds. C. S. Wong, E. Boyle, K. W. Bruland, J. D. Burton and E. D. Goldberg). Springer, US, Boston, MA, pp. 643–669.
Paulukat C., Døssing L. N., Mondal S. K., Voegelin A. R. and Frei R. (2015) Oxidative release of chromium from Archean ultramafic rocks, its transport and environmental impact – A Cr isotope perspective on the Sukinda valley ore district (Orissa, India). *Appl. Geochem.* **59**, 125–138.
Paulukat C., Gilleaudeau G. J., Chernyavskiy P. and Frei R. (2016) The Cr-isotope signature of surface seawater — A global perspective. *Chem. Geol.* **444**, 101–109.
Pennington J. T., Mahoney K. L., Kuwahara V. S., Kolber D. D., Calienes R. and Chavez F. P. (2006) Primary production in the eastern tropical Pacific: a review. *Prog. Oceanogr.* **69**, 285–317.
Penven P., Echevin V., Pasapera J., Colas F. and Tam J. (2005) Average circulation, seasonal cycle, and mesoscale dynamics of the Peru Current System: a modeling approach. *J. Geophys. Res. Ocean.* **110**.
Pettine M. (2000) Redox processes of chromium in sea water. In *Chemical Processes in Marine Environments* (eds. A. Gianguzza, E. Pelizzetti and S. Sammertano). Springer, Berlin, pp. 281–296.
Pettine M., Millero F. J. and Passino R. (1994) Reduction of chromium (VI) with hydrogen sulfide in NaCl media. *Mar. Chem.* **46**, 335–344.
Planavsky N. J., Reinhard C. T., Wang X., Thomson D., McGoldrick P., Rainbird R. H., Johnson T., Fischer W. W. and Lyons T. W. (2014) Low Mid-Proterozoic atmospheric oxygen levels and the delayed rise of animals. *Science* **346**, 635–638.

Qin L. and Wang X. (2017) Chromium isotope geochemistry. *Rev. Mineral. Geochem.* **82**, 379–414.

Quinby-Hunt M. S. and Turehian K. K. (1983) Distribution of elements in sea water. *Eos Trans. Am. Geophys. Union* **64**, 130.

Rai D., Eary L. E. and Zachara J. M. (1989) Environmental chemistry of chromium. *Sci. Total Environ.* **86**, 15–23.

Reinhard C. T., Planavsky N. J., Wang X., Fischer W. W., Johnson T. M. and Lyons T. W. (2014) The isotopic composition of authigenic chromium in anoxic marine sediments: a case study from the. *Cariaco Basin.*.

Rickli J., Janssen D. J., Hassler C., Ellwood M. J. and Jaccard S. L. (2019) Chromium biogeochemistry and stable isotope distribution in the Southern Ocean. *Geochim. Cosmochim. Acta* **262**, 188–206.

Rue E. L., Smith G. J., Cutter G. A. and Bruland K. W. (1997) The response of trace element redox couples to suboxic conditions in the water column. *Deep Sea Res. Part I Oceanogr. Res. Pap.* **44**, 113–134.

Saad E. M., Wang X., Planavsky N. J., Reinhard C. T. and Tang Y. (2017) Redox-independent chromium isotope fractionation induced by ligand-promoted dissolution. *Nat. Commun.* **8**, 1590.

Sander S. and Koschinsky A. (2000) Onboard-ship redox speciation of chromium in diffuse hydrothermal fluids from the North Fiji Basin. *Mar. Chem.* **71**, 83–102.

Schauble E. A. (2004) Applying stable isotope fractionation theory to new systems. *Rev. Mineral. Geochem.* **55**, 65–111.

Schauble E., Rossman G. R. and Taylor H. P. (2004) Theoretical estimates of equilibrium chromium-isotope fractionations. *Chem. Geol.* **205**, 99–114.

Scheiderich K., Amini M., Holmden C. and Francois R. (2015) Global variability of chromium isotopes in seawater demonstrated by Pacific, Atlantic, and Arctic Ocean samples. *Earth Planet. Sci. Lett.* **423**, 87–97.

Schlosser C. and Croot P. L. (2019) Trace metal concentration from water samples during METEOR cruise M77/3. Suppl. to Schlosser, Christ. Streu, Peter; Frank, Martin; Lavik, Gaute; Croot, Peter L; Dengler, Marcus; Achterberg, Eric Pieter H2S events Peruvian Oxyg. Minim. Zo. Facil. Enhanc. dissolved Fe Conc. Sci. Rep.

Schlosser C., Streu P., Frank M., Lavik G., Croot P. L., Dengler M. and Achterberg E. P. (2018) H2S events in the Peruvian oxygen minimum zone facilitate enhanced dissolved Fe concentrations. *Sci. Rep.* **8**, 12642.

Schoenberg R., Zink S., Staubwasser M. and von Blanckenburg F. (2008) The stable Cr isotope inventory of solid Earth reservoirs determined by double spike MC-ICP-MS. *Chem. Geol.* **249**, 294–306.

Scholz F., Severmann S., McManus J. and Hensen C. (2014) Beyond the Black Sea paradigm: the sedimentary fingerprint of an open-marine iron shuttle. *Geochim. Cosmochim. Acta* **127**, 368–380.

Schunck H., Lavik G., Desai D. K., Großkopf D. K., Kalvelage T. and Löscher C. R. (2013) Giant hydrogen sulfide plume in the oxygen minimum zone off Peru supports chemolithoautotrophy. *PLoS One* **8** e68661.

Semeniuk D. M., Maldonado M. T. and Jaccard S. L. (2016) Chromium uptake and adsorption in marine phytoplankton - Implications for the marine chromium cycle. *Geochim. Cosmochim. Acta* **184**, 41–54.

Silva N., Rojas N. and Fedele A. (2009) Water masses in the Humboldt Current System: properties, distribution, and the nitrate deficit as a chemical water mass tracer for Equatorial Subsurface Water off Chile. *Deep Res. Part II Top. Stud. Oceanogr.* **56**, 992–1008.

Sirinawin W., Turner D. R. and Westerlund S. (2000) Chromium (VI) distributions in the Arctic and the Atlantic Oceans and a reassessment of the oceanic Cr cycle. *Mar. Chem.* **71**, 265–282.

Thamdrup B., Dalsgaard T. and Revsbech N. P. (2012) Widespread functional anoxia in the oxygen minimum zone of the Eastern South Pacific. *Deep Sea Res. Part I Oceanogr. Res. Pap.* **65**, 36–45.

Toggweiler J. R., Dixon K. and Broecker W. S. (1991) The Peru upwelling and the ventilation of the south Pacific thermocline. *J. Geophys. Res.* **96**, 20467.

Whitfield M. and Turner D. R. (1987) The role of particles in regulating the composition of seawater. In *Aquatic Surface Chemistry* (ed. W. Stumm). Wiley-Interscience, New York, pp. 457–493.

Winkler L. W. (1888) Die Bestimmung des im Wasser gelösten Sauerstoffes. *Berichte der Dtsch. Chem. Gesellschaft* **21**, 2843–2854.

Wyrtki K. (1967) Circulation and water masses in the eastern equatorial pacific ocean. *Int. J. Oceanol. Limnol.* **1**, 117–147.

Yamakawa A., Yamashita K., Makishima A. and Nakamura E. (2009) Chemical separation and mass spectrometry of Cr, Fe, Ni, Zn, and Cu in terrestrial and extraterrestrial materials using thermal ionization mass spectrometry. *Anal. Chem.* **81**, 9787–9794.

Zink S., Schoenberg R. and Staubwasser M. (2010) Isotopic fractionation and reaction kinetics between Cr(III) and Cr(VI) in aqueous media. *Geochim. Cosmochim. Acta* **74**, 5729–5745.

Associate editor: Rachael James